A Printed Leaky-Wave Antenna Based on a Sinusoidally-Modulated Reactance Surface

Amit M. Patel, *Student Member, IEEE*, and Anthony Grbic, *Member, IEEE*

***Abstract*—A simple procedure for designing a sinusoidally-modulated reactance surface (SMRS) that radiates at an arbitrary off-broadside angle is outlined. The procedure allows for nearly independent control of the leakage and phase constants along the surface. Printing an array of metallic strips over a grounded dielectric substrate is discussed as a way to practically implement the theoretical SMRS. A method of mapping the gaps between metallic strips to a desired surface impedance is presented as an efficient alternative to mapping methods used in the past. A printed leaky-wave antenna with a sinusoidally-modulated surface reactance is designed using the procedure mentioned above. The TM-polarized antenna radiates at 30° from broadside at 10 GHz, and exhibits an experimental gain of 18.4 dB. Theoretical, simulated, and experimental results are presented.**

***Index Terms*—Leaky wave antennas, leaky waves, microstrip antennas, periodic structures, surface waves.**

I. Introduction

In recent years, there has been strong interest in high gain, low profile antennas that can be easily integrated into the surfaces of vehicles or other platforms [1]–[4]. Planar leaky-wave antennas are excellent candidates for this purpose as they leak power from traveling waves propagating along the antenna surface. They are typically characterized by a phase and leakage constant along the antenna. Independent control over these two leaky-wave parameters is highly desired since it allows beam shaping [5].

Electromagnetic propagation along a sinusoidally-modulated reactance surface (SMRS) was theoretically investigated by A. A. Oliner in 1959 as a way to increase the gain of surface-wave antennas [6]. More recently, SMRSs have been used to develop holographic antennas [7]–[9], which use the interference pattern between the field of a source and the desired radiated field to establish a sinusoidally varying surface impedance. These holographic antennas have shown great promise, but literature explaining their design has been limited. Furthermore, since many of these antennas are reflectors, they need to be illuminated by a separate radiator such as a horn antenna or waveguide aperture. A direct feeding solution would be desirable for many applications. Slotted parallel-plate waveguides have been used extensively as leaky-wave antennas, since they are simple to fabricate and feed. However, they lack the independent control over phase and attenuation constants [10]–[12] that SMRSs provide.

In this paper, we outline a step-by-step procedure for designing an SMRS that radiates at a desired angle. The concepts of an SMRS and a periodically slotted parallel-plate waveguide antenna are then combined to design a printed leaky-wave antenna that possesses a sinusoidally varying surface reactance [13]. The antenna is directly fed, simple to fabricate and allows for nearly independent control of phase and attenuation constants.

In Section II, an overview of sinusoidally-modulated reactance surfaces and related theory is presented. The step-by-step design procedure for designing a SMRS with desired radiation characteristics is discussed in Section III. A detailed example is also presented in this section. Section IV shows how the designed SMRS can be used to realize a leaky-wave antenna by printing metallic strips (separated by varying gaps) over a grounded dielectric substrate. A method for determining the appropriate gap sizes is outlined. Finally, Section V reports simulation and experimental results for the antenna.

II. Theory

A sinusoidally-modulated reactance surface refers to a surface whose modal surface impedance is modulated sinusoidally. The modal surface impedance is defined as the ratio of the tangential electric field to the tangential magnetic field of the surface wave guided by the reactance surface. By convention, the surface impedance is defined such that the Poynting vector points into the surface. Since the modal surface impedance (η_{surf}) is modulated sinusoidally, three parameters (X, M, a) can be used to characterize it (Fig. 1). The average surface reactance will be denoted by X, the modulation factor by M, and the periodicity of the sinusoid by a. In the cases considered in this paper, η_{surf} will be inductive such that it supports a TM surface wave [14]. The z-direction will be assumed to be the direction of propagation along the SMRS. The surface impedance is given by the following expression

$$\eta_{surf}(z) = j\eta_0 X' \left[1 + M\cos\left(\frac{2\pi z}{a}\right)\right] \tag{1}$$

where X' is the average surface reactance normalized by the free-space wave impedance $(X' = X/\eta_0)$.

Due to the periodic nature of the surface impedance, the fields above the surface can be expanded in terms of spatial harmonics, as shown in Fig. 2. The fundamental wave number tangential to

Manuscript received March 02, 2010; revised October 13, 2010; accepted January 15, 2011. Date of publication April 19, 2011; date of current version June 02, 2011. This work was supported in part by a Presidential Early Career Award for Scientists and Engineers (FA9550-09-1-0696), an NSF Faculty Early Career Development Award (ECCS-0747623) and in part by an AFOSR Young Investigator Research Program Award (FA9550-08-1-0067).

The authors are with the Radiation Laboratory, Department of Electrical Engineering and Computer Science, University of Michigan-Ann Arbor, Ann Arbor, MI 48109-2122 USA (e-mail: agrbic@umich.edu).

Color versions of one or more of the figures in this paper are available online at http://ieeexplore.ieee.org.

Digital Object Identifier 10.1109/TAP.2011.2143668

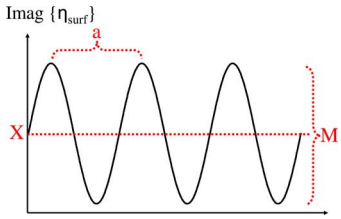

Fig. 1. Sinusoidal form of the surface reactance.

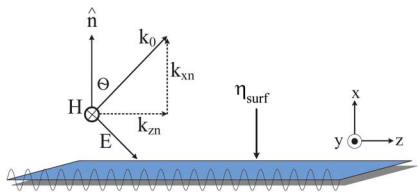

Fig. 2. Spatial harmonic representation of fields due to SMRS and their corresponding wave numbers.

the surface (Bloch wave number) will be written as $k_{z0} = \kappa$ and the tangential wave number of the nth spatial harmonic as $k_{zn} = \kappa + 2\pi n/a$. The corresponding normal wave numbers (k_{xn}) can be found using the separation relation

$$k_{xn} = \sqrt{k_0^2 - \left(\kappa + \frac{2\pi n}{a}\right)^2}. \tag{2}$$

Employing the definition of surface impedance and (1), a dispersion relation can be written in continued fraction form [6]:

$$\begin{aligned} 1 - \frac{j}{X'}\sqrt{1-\left[\frac{\kappa}{k_0}\right]^2} &= \cfrac{M^2/4}{1 - \frac{j}{X'}\sqrt{1-\left[\frac{\kappa}{k_0}+\frac{2\pi(-1)}{k_0 a}\right]^2}} \\ &\quad - \cfrac{M^2/4}{1 - \frac{j}{X'}\sqrt{1-\left[\frac{\kappa}{k_0}+\frac{2\pi(-2)}{k_0 a}\right]^2}} \cdots \\ &\quad + \cfrac{M^2/4}{1 - \frac{j}{X'}\sqrt{1-\left[\frac{\kappa}{k_0}+\frac{2\pi(1)}{k_0 a}\right]^2}} \\ &\quad - \cfrac{M^2/4}{1 - \frac{j}{X'}\sqrt{1-\left[\frac{\kappa}{k_0}+\frac{2\pi(2)}{k_0 a}\right]^2}} \cdots, \end{aligned} \tag{3}$$

where $\kappa = \beta - j\alpha$.

Explicit expressions for the relative amplitudes of the magnetic-field spatial harmonics have also been derived in [6]. Equation (3) is a function of κ, the primary quantity of interest. Once κ is known, all of the spatial harmonic wave numbers are known, and the relative amplitudes of the spatial harmonics can be calculated. Solving (3) numerically for κ, for the case $X' = 1.2$ and $M = 0.2$, yields the dash-dot curve shown in Fig. 3. Notice the appearance of the stop band and the higher-order spatial harmonics (dashed curves). It should

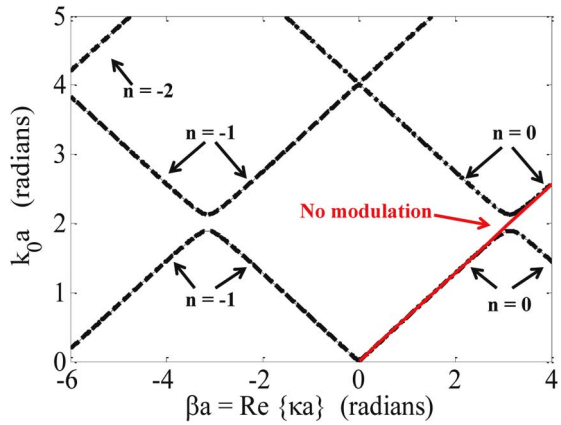

Fig. 3. Solution of dispersion (3) for varying periodicity (κa versus $k_0 a$ for $X = 1.2$, $M = 0.2$).

be noted that if (3) was solved for the case of no modulation $(M = 0)$, the equation would simplify to

$$\kappa = k_0\sqrt{1 + X'^2} \tag{4}$$

and the solution would be given by the solid line in Fig. 3. For small values of modulation ($M = 0.2$ in this case), the full solution for κ obtained from (3) can be approximated by the solution of κ obtained from (4). Since (4) assumes no modulation, it is only valid away from the stop bands. Furthermore, it is evident that (4) is not a periodic function so it will not yield a periodic solution. Its solution will only yield an approximation for the fundamental wave number along the surface and not for the higher-order spatial harmonics. However, since the higher-order spatial harmonics are simply shifted versions of the fundamental harmonic, it is still possible to approximate the higher-order spatial harmonics with shifted versions of the unmodulated solution. These approximate solutions will be exploited to construct a simplified design procedure.

III. Surface Design

A. Simplified Design Procedure

This section outlines a step-by-step procedure for designing a sinusoidally-modulated reactance surface that radiates at an arbitrary off-broadside angle. Specifically, a procedure is outlined that describes how the parameters X, M, and a can be selected to generate directive radiation at a desired angle for a fixed frequency. The fundamental wave number along the surface can be decomposed into its real and imaginary parts, $\kappa = \beta - j\alpha$, where β represents the propagation constant (or phase delay) and α represents the attenuation constant (or leakage rate) along the surface. For the unmodulated case $(M = 0)$, the dispersion equation reduces to

$$\kappa_{approx} = k_0\sqrt{1 + X'^2} = \beta_{approx} \tag{5}$$

where β_{approx} is close to the actual value of β when the modulation of the surface is small. Since (5) only yields real solutions, κ_{approx} will only yield a real-valued approximation for

κ, implying that there is a phase delay along the surface (β is non-zero) but no attenuation due to radiation ($\alpha = 0$). In reality, κ will be complex, since leaky waves can be excited. This will be reconciled later in the design process. The design process can be broken down into ten steps, which are outlined below.

1) Choose a design frequency (f_0) and its corresponding free space wave number, $k_0 = 2\pi f_0/c$.
2) Choose the desired angle of radiation for the $n = -1$ spatial harmonic ($\theta_{n=-1}$) such that $90^\circ > \theta_{n=-1} > -90^\circ$.
3) Fix the value of either X (average surface reactance) or a (periodicity).
4) Solve for the remaining value using

$$\sin(\theta_{n=-1}) \approx \sqrt{1 + X'^2} - \frac{2\pi}{k_0 a}. \tag{6}$$

5) Solve for β_{approx} using

$$\sin(\theta_{n=-1}) = \frac{\beta_{approx} - \frac{2\pi}{a}}{k_0}. \tag{7}$$

Equation (7) is derived from (5), which assumes that $M = 0$. In reality, $M \neq 0$, but this assumption allows for an approximate β (denoted by β_{approx}) to be computed, since low values of modulation only perturb β slightly from the unmodulated case. The choice of X and a predominately determines β, and therefore the beam direction [5].

6) Choose a value for M, where $M \leq 1$. A non-zero modulation introduces an attenuation constant α and the wave number along the surface (κ) becomes complex.
7) (Optional) Compute a more accurate value of κ, including the imaginary component, by using the full dispersion (3) if M is large. The following perturbation equation can be used for small values of M [6].

$$\begin{aligned}\kappa &= \beta - j\alpha \\ &= k_0\sqrt{1 + X'^2} \\ &\quad - \frac{M^2}{4}\frac{k_0 X'^2}{\sqrt{1 + X'^2}} \\ &\quad \times \left[\frac{1}{1 - \frac{j}{X'}\sqrt{1 - \left[\sqrt{1 + X'^2} - \frac{2\pi}{k_0 a}\right]}}\right. \\ &\quad \left. + \frac{1}{1 - \frac{j}{X'}\sqrt{1 - \left[\sqrt{1 + X'^2} + \frac{2\pi}{k_0 a}\right]}}\right].\end{aligned} \tag{8}$$

The variables X and a control β (beam direction), while M controls the attenuation constant (antenna beam width). Larger values of M lead to larger values of α and therefore broader beam widths. A distribution of α can be used to control side lobe levels of the radiation pattern [5]. This can be achieved by varying M along the antenna [15].

There are two advantages to dealing with low values of modulation. Firstly, the design procedure can be simplified significantly since the $M = 0$ approximation can be used away from stop bands. This removes the need for iteratively solving the dispersion (3). Secondly, the beam direction can be designed by determining X and a, and the beam width controlled by adjusting M without significantly altering the beam direction. This allows for nearly independent control of α and β. The definition of "low" values of modulation will be discussed in Section III-B.

8) For the case where the accuracy of the beam direction is critical, the slight beam-shift that occurs due to the introduction of M can be compensated for with a slight adjustment of X.
9) Verify that the operating point $k_0 a$ is not in the band-gap for the selected values of X, M, and a.
10) Finally, check if there are other radiating spatial harmonics besides the $n = -1$ harmonic. The nth harmonic will radiate at an angle

$$\theta_n = \arcsin\left(\frac{\kappa a + 2\pi n}{k_0 a}\right) \tag{9}$$

when

$$\left(\kappa + \frac{2\pi n}{a}\right)^2 < k_0. \tag{10}$$

In Section III-B, this ten step procedure is used to design a surface that radiates at 30°.

B. Surface Design for 30° Main Beam at 10 GHz

A surface was designed that radiates at an angle of $\theta_{n=-1} = 30^\circ$ from broadside at an operating frequency of 10 GHz. Using the design procedure described above, this surface was designed with the parameters $X' = 1.2$, $M = 0.2$, $a = 28.25$ mm. Fig. 4 shows the Brillouin diagram for the structure. The solid lines are light lines and define the radiation cone. The fundamental harmonic never penetrates the radiation cone and therefore is always bound to the surface. Point A represents the point where the $n = -1$ spatial harmonic enters the radiation cone (backward endfire). Point B is where it radiates in the broadside direction and point C (shown as an inset in Fig. 4) is where the $n = -1$ spatial harmonic exits the radiation cone, representing forward endfire. Therefore, points A and C mark the operating boundaries of the antenna. It should be noted that a directive beam cannot be designed exactly at broadside due to a dramatic increase in the attenuation constant at this point [16]. At the operating point of $k_0 a = 5.917$ radians, the $n = -1$ spatial harmonic radiates at $\theta_{n=-1} = 30^\circ$, verifying the design procedure. A parasitic beam from the $n = -2$ spatial harmonic is also present at $\theta_{n=-2} = -34.18^\circ$. These angles can easily be calculated using (9). Calculating the radiation angle for the other spatial harmonics will show that $\theta_{n=0,1,2\ldots} \approx 90^\circ$ and $\theta_{n=-3,-4,-5,\ldots} \approx -90^\circ$ corresponding to forward-bound and backward-bound waves, respectively. This is consistent with the Brillouin diagram of Fig. 4 with regard to which spatial harmonics appear in the radiation cone.

Figs. 5 and 6, generated using (4), show the dependence of α and β on the modulation factor when $X' = 1.2$ is fixed and $k_0 a = 5.917$ radians is fixed. For low values of modulation,

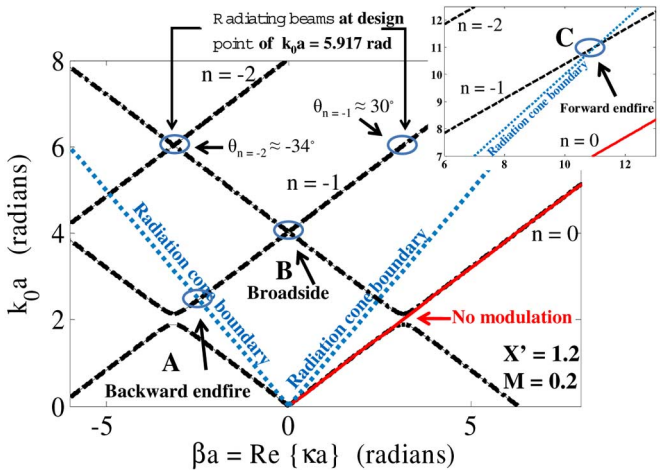

Fig. 4. Brillouin diagram for a SMRS with design parameters: $X = 1.2, M = 0.2$.

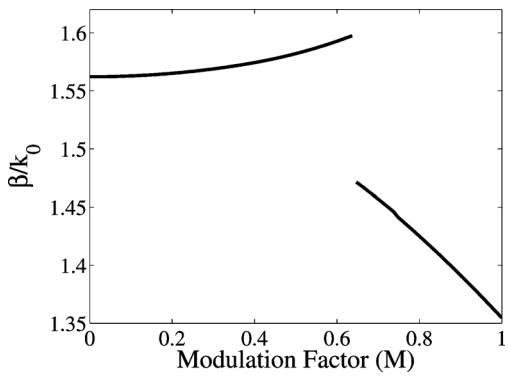

Fig. 5. Theoretical variation in normalized propagation constant (β/k_0) along an ideal SMRS as a function of modulation (M) for $X' = 1.2$ and $k_0a = 5.917$ radians.

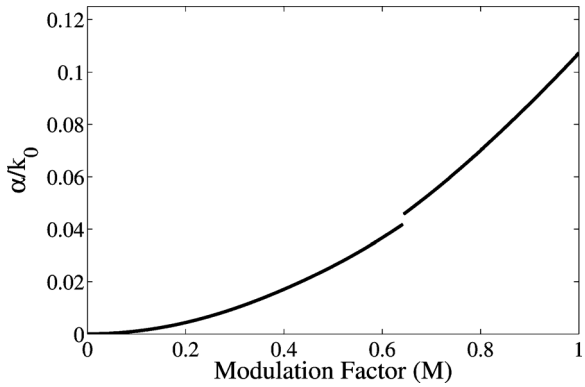

Fig. 6. Theoretical variation in normalized attenuation constant (α/k_0) along an ideal SMRS as a function of modulation (M) for $X' = 1.2$ and $k_0a = 5.917$ radians.

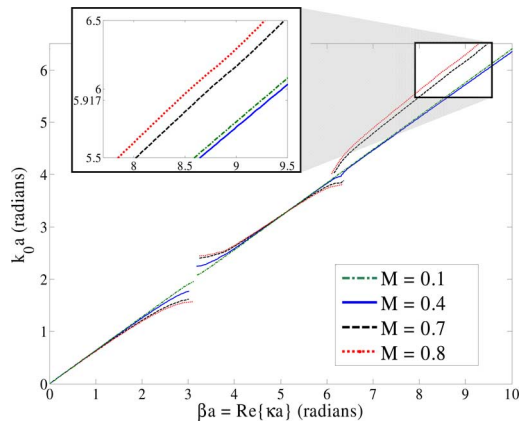

Fig. 7. Band diagram showing the effect of increasing modulation while keeping $X' = 1.2$ fixed. At the fixed value of $k_0a = 5.917$ radians, β will first increase and then decrease as modulation increases (inset).

($M < 0.6$ in this case), it is clear that α changes dramatically whereas β is only slightly perturbed. This demonstrates nearly independent control of the parameters over a fairly wide range of modulation factor, M. The range over which β remains fairly constant determines the values of M are considered to be "low". Fairly independent control of α and β can be achieved for values of modulation up to $M \approx 0.6$. The sudden change in β that occurs when $M \approx 0.6$ can also be seen in the band diagrams shown in Fig. 7 for four different modulation factors. For the designed surface with $M = 0.2$, the surface impedance ranges between $361.92j\ \Omega$ and $542.88j\ \Omega$. The impedance range corresponding to $M = 0.6$ is $180.96j\ \Omega$ to $723.84j\ \Omega$. Therefore, even "low" values of modulation correspond to fairly wide impedance ranges. Now that a theoretical surface possessing the desired radiation characteristics has been designed, the question remains as to how this surface can be implemented and a leaky-wave antenna made from it. The Section IV will address these questions.

IV. Leaky-Wave Antenna Implementation

A. From a Theoretical Surface to a Realizable Antenna

Thus far, the discussion has been restricted to SMRSs and the design procedure for one that radiates the $n = -1$ spatial harmonic at a specified angle. In the previous section, a surface was designed to radiate a beam at $\theta_{n=-1} = 30°$ at a frequency of 10 GHz. This section will describe the implementation of this SMRS using a printed circuit board, in order to create a leaky-wave antenna that radiates at the same angle and frequency as the theoretical surface.

The SMRS was implemented as an array of copper strips over a grounded dielectric substrate, as shown in Fig. 8. One period (a) of the sinusoidal surface impedance will be referred to as a unit cell. Each unit cell was implemented by sampling the surface impedance at ten discrete, equispaced points. The impedance at each point was realized as a gap between two copper strips over a grounded dielectric substrate. The strips were printed onto an ARLON AD-600 substrate $(\epsilon_r = 6.15, tan\delta \approx 0.0035)$ with thickness $d = 2.54$ mm using a photolithographic etching procedure. The array of strips was designed to have periodically varying gaps to achieve the sinusoidal, modal surface impedance profile needed to realize the SMRS. The antenna, consisting of approximately eight unit cells, was 22.88 cm in length. The width of the surface was truncated (to 30 mm), such that a fairly uniform aperture illumination was still present, forming a leaky-wave antenna. The method used to map a certain gap-size to a desired surface impedance will be described in detail in Section IV-B.

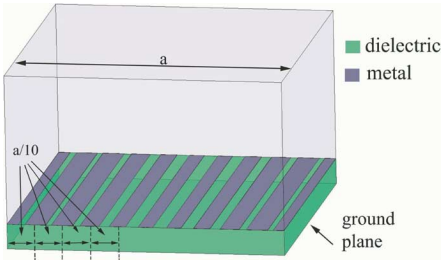

Fig. 8. Unit cell representing one period of the SMRS.

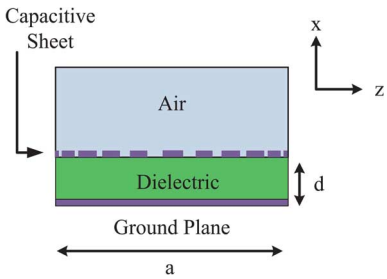

Fig. 9. Side view of one unit cell representing one period of the SMRS.

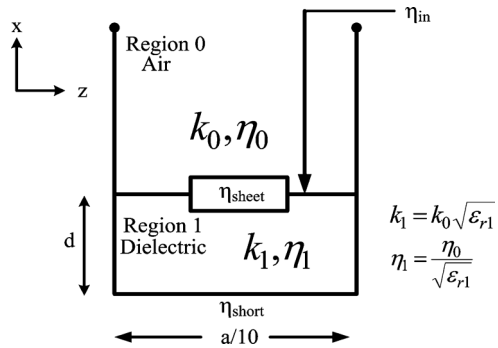

Fig. 10. Normal-incidence transmission-line model for one discrete segment of the unit cell.

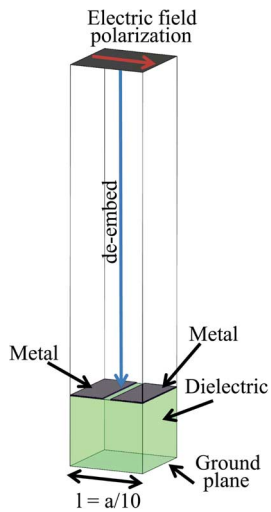

Fig. 11. The normal-incidence scattering simulation performed on a single gap (segment) in order to find η_{in} and the extracted sheet impedance (η_{sheet}).

B. Mapping Surface Impedance to Gap Size

The SMRS was implemented as a multi-layer structure consisting of a periodically varying capacitive sheet (metallic strips) over a grounded dielectric substrate. A unit cell, corresponding to one period of the sinusoidal surface impedance, is shown in Fig. 9. The capacitive sheet was designed such that the modal surface impedance looking into the multi-layer structure has the same sinusoidal η_{surf} as the theoretical SMRS designed in Section III. Each period (a) of the capacitive sheet was discretized into ten segments ($a/10$ in size). The capacitance over each segment was assumed to be constant, and was implemented as two copper strips separated by a gap. The capacitance of each segment is represented by a constant sheet impedance, η_{sheet}, shown in Fig. 10. This sheet impedance is defined as the ratio of the tangential electric field to the surface current on the sheet. The sheet impedance, which is in parallel with a short-circuited transmission line (representing the grounded dielectric substrate with thickness d) constitutes the transmission-line model of each segment. The transmission-line model of each segment (Fig. 10) is first used to find η_{sheet} from normal-incidence scattering simulations. This sheet impedance is then used to find the TM modal surface impedance (η_{surf}) for that specific gap size. It should be noted that a pole-zero representation of η_{sheet} as a function of β and frequency has been presented in [17], which is valid for complex geometries over a wide range of frequencies and incident angles. The overall goal here is to find the mapping between gap size and η_{surf}, so that a desired surface impedance profile can be realized by printing an array of metallic strips with varying gaps over a grounded dielectric substrate. Details of the procedure are outlined below.

1) The first step is to find the input impedance, η_{in}, of a single gap over the grounded dielectric substrate at normal incidence. This is accomplished by performing a simple normal-incidence scattering simulation, such as a driven-mode simulation in Ansoft HFSS (see Fig. 11). The smallest gap allowed by one's fabrication facility marks a good starting point. Since η_{in} is based on normal incidence, there is no phase delay along the surface and therefore no information can be gathered regarding the modal impedance of a surface wave that can be guided. However, it is still possible to extract η_{sheet} from η_{in}.
2) Using the circuit model shown in Fig. 10, η_{sheet} can be extracted using the following expression:

$$\frac{1}{\eta_{sheet}} = \frac{1}{\eta_{in}} - \frac{1}{j\eta_1 \tan(k_1 d)} = \frac{1}{\eta_{in}} - \frac{1}{j\frac{\eta_0}{\sqrt{\epsilon_{r1}}} \tan(k_0\sqrt{\epsilon_{r1}} d)}. \quad (11)$$

The characteristic wave numbers and impedances in the transmission-line model are just those of free space in region 0 and the dielectric substrate with permittivity ϵ_{r1} in region 1, respectively.
3) Once η_{sheet} is determined, it is possible to find η_{surf} by using a modified transmission-line model where the characteristic wave numbers and impedances are now represented by the TM wave numbers and impedances, as shown in Fig. 12. From this transmission-line model, it is apparent

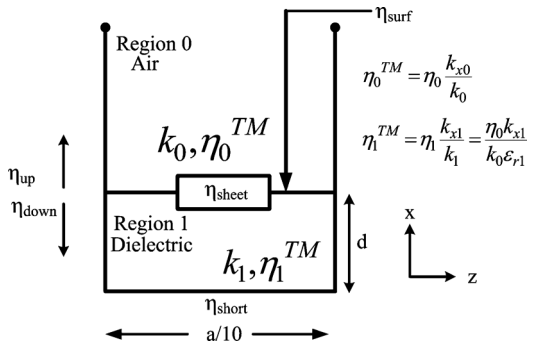

Fig. 12. Modified transmission-line model for deriving the modal impedance.

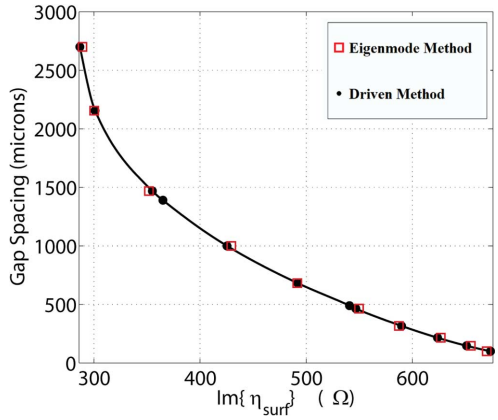

Fig. 13. Gap spacing vs. surface reactance for the designed antenna. For the driven method, the sheet impedance is extracted from normal-incidence scattering simulations.

that η_{surf} is given by the impedance looking down into the shunt combination of η_{sheet} and a transmission-line section representing the grounded dielectric substrate with thickness d. The transverse resonance technique [5] can be applied to derive a dispersion equation for the TM surface waves guided by this multi-layer structure. Considering the transmission-line model shown in Fig. 12,

$$\frac{1}{\eta_{up}(z)} + \frac{1}{\eta_{down}(z)} = 0 \tag{12}$$

where η_{up} and η_{down} represent the impedances looking in opposite directions from any point on the transmission line. In this case, it is appropriate to use the impedances observed above and below the capacitive sheet, as shown in Fig. 12. The dispersion relation from (12) can be written as

$$\frac{1}{\eta_{surf}} = \frac{1}{\eta_{sheet}} + \frac{1}{j\frac{\eta_0 k_{x1}}{k_0 \epsilon_{r1}} \tan(k_{x1} d)} \tag{13}$$

where

$$k_{x1} = \sqrt{k_0^2(\epsilon_{r1} - 1) + \left(\frac{\eta_{surf} k_0}{\eta_0}\right)^2}. \tag{14}$$

This equation can be solved numerically to find η_{surf}, from η_{sheet} extracted for a given gap size.

4) Since the gap size is a free parameter, a design curve can be generated by parametrically sweeping the gap size in simulation and repeating the above procedure for the various gap sizes. A curve can be fitted to the data points to create a design curve which maps desired surface impedance values to the gap sizes needed to achieve them.

Fig. 13 represents the design curve used to map a desired surface impedance to its corresponding gap size for the antenna designed in this paper.

Methods used in the past for relating gap size to η_{surf} included using an eigenmode simulator to parametrically sweep not only gap size, but also phase delay [7], [8]. For a given gap size, the phase delay across the unit cell needed to be swept in order to find the phase delay that corresponds to the operating frequency. Once this phase delay was found (for a given gap size) the surface impedance could be computed using [7]

$$\eta_{surf} = j\eta_0 \sqrt{\left(\frac{\phi}{k_0 l}\right)^2 - 1} \tag{15}$$

where ϕ represents the phase delay across the unit cell and $l = a/10$ represents the width of one-tenth of a unit cell, as shown in Fig. 11. This procedure had to be repeated for each gap size resulting in time consuming, two-dimensional sweeps over phase delay and gap size. Other methods include using custom MoM or FEM eigenmode solvers to numerically solve for phase delay across the periodic unit cell for a stipulated frequency. Equation (15) assumes that the segment, consisting of a multi-layer structure (capacitive sheet over a grounded dielectric substrate), can be approximated as a surface impedance. As will be shown in Section V, this approximation does not allow the attenuation constant to be predicted accurately if the net thickness of the multi-layer structure is not very small compared to a wavelength.

The main advantage of the method proposed in this paper is that simulations can be done easily using a commercial solver. Furthermore, the commercial solver can be operated in scattering-solution mode, as opposed to eigen-solution mode. This eliminates the ambiguity of multiple modes corresponding to a single phase delay across the cell. In the method proposed in this paper, only the gap size parameter needs to be swept, therefore significantly reducing the number of time consuming simulations that need to be performed. Fig. 13 compares the design curves generated using the eigenmode method [7] and the driven method proposed in this paper. Close agreement between the two methods is observed.

The driven method assumes that the only interaction between the ground plane and the capacitive sheet is via propagating waves through the dielectric. It should be noted that the method is strictly valid when the dielectric thickness, d, is larger than the widest gap-size. This ensures that the evanescent wave interaction between the ground plane and the capacitive sheet is minimal [18].

Fig. 14. Photograph of fabricated antenna with a 50 Ω termination at one end.

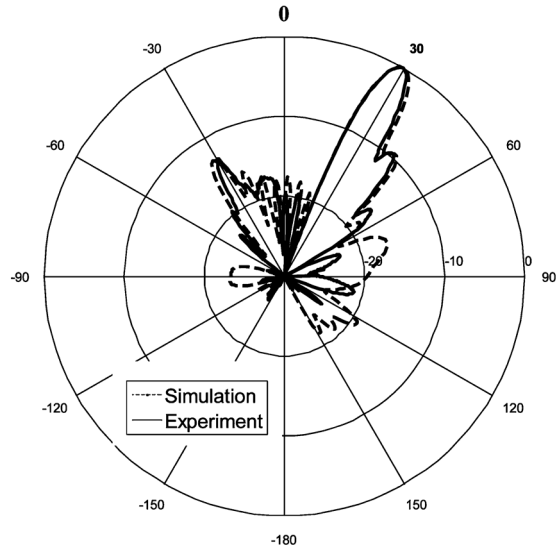

Fig. 15. Simulated and measured co-polarization E-plane radiation patterns at $f_0 = 10$ GHz.

V. Simulation and Experiment

A leaky-wave antenna, consisting of eight unit cells, was designed according to the procedure outlined in the previous section. Both ends of the antenna were tapered down to 50 Ω microstrip transmission lines and connected to edge-mount SMA connectors (see Fig. 14). This allowed return loss and insertion loss measurements to be performed. The tapers provided a transition between the antenna and the 50 Ω feed lines, providing an impedance match. During the radiation pattern measurements, the antenna was fed at one end while the other was terminated with a 50 Ω SMA load to minimize reflections from the end of the antenna.

Fig. 15 shows good correspondence between the simulated (using Ansoft HFSS) and measured radiation patterns along the E-plane, at the design frequency of 10 GHz. The angles of maximum radiation for the simulated and fabricated antennas were 30° and 29.25° respectively. The simulated HPBW along the E-plane was 8.51° in simulation and 7.57° in experiment. The simulated and measured gains were 17.04 dB and 18.4 dB respectively, and the measured cross-polarization remained below -22 dB over all angles, as seen in Fig. 16. The return loss and insertion loss from 9 GHz to 11 GHz is shown in Fig. 17. It should be noted that due to the complexity of the full-wave simulation, which involved a multiple wavelength long structure with many sub-wavelength features, the simulation did not reach a high level of convergence. This accounts for the lower gain from simulation compared to that from experiment.

The radiation patterns were also measured at discrete frequencies between 9 GHz and 11 GHz. Fig. 18 shows co-polarization and cross-polarization radiation patterns at 0.5 GHz increments between 9 GHz and 11 GHz, while Fig. 19 shows the simulated patterns versus the measured ones. The average beam squint was approximately 17.5°/GHz and the beam angle was $\approx$ 13° and $\approx$48° at 9 GHz and 11 GHz respectively. The directions and beam widths of the measured main beams were in close agreement with the simulated patterns.

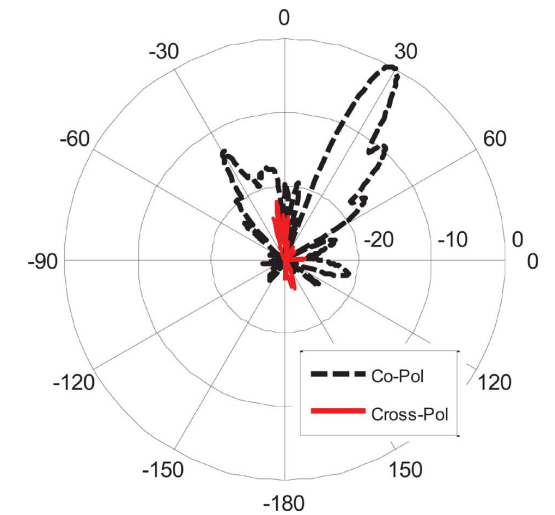

Fig. 16. Measured co-polarization and cross-polarization E-plane radiation patterns at $f_0 = 10$ GHz.

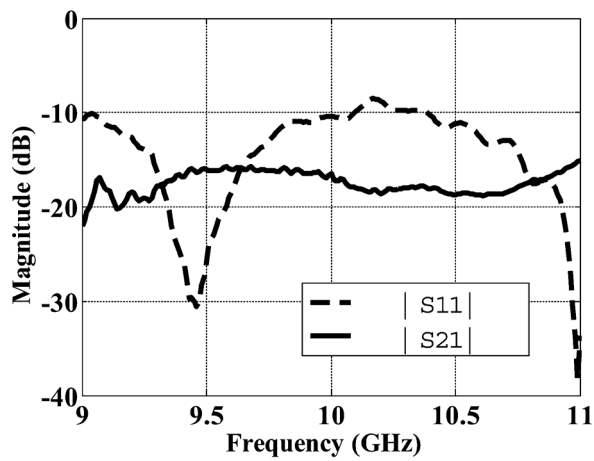

Fig. 17. Measured $|S11|$ and $|S21|$ from 9 GHz to 11 GHz.

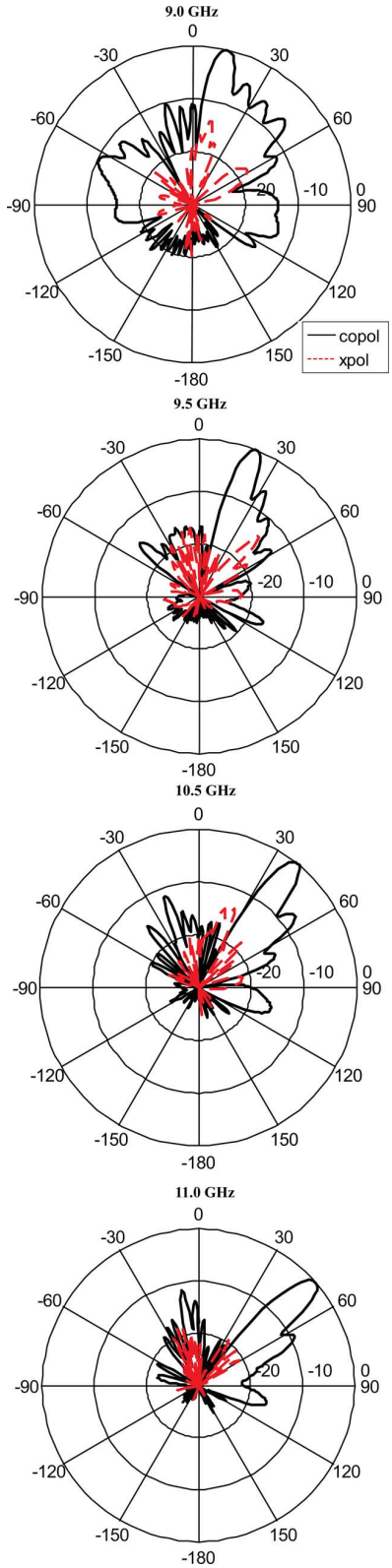

Fig. 18. Measured co-polarization and cross-polarization E-plane radiation patterns for various frequencies between 9 GHz and 11 GHz.

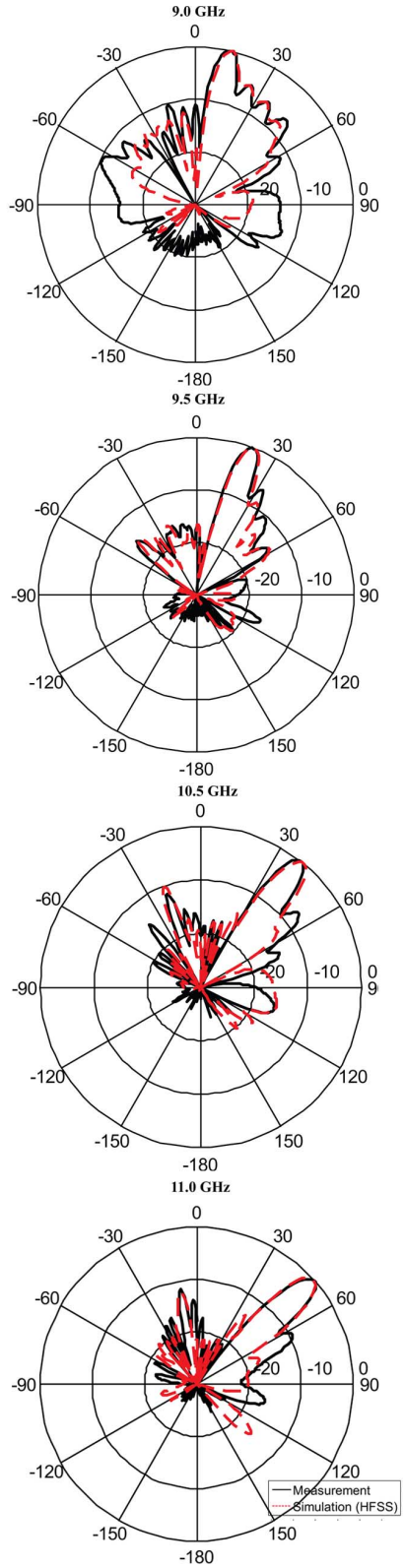

Fig. 19. Measured and simulated co-polarization E-plane radiation patterns for frequencies between 9 GHz and 11 GHz.

At the design frequency, the beam angle was very close to the design angle of 30°, showing that the implemented SMRS was able to realize β accurately. However, based on the beam width of the main beam in Fig. 15, the value of α for the implemented SMRS was significantly larger than that predicted by SMRS theory. Due to fabrication constraints on minimum

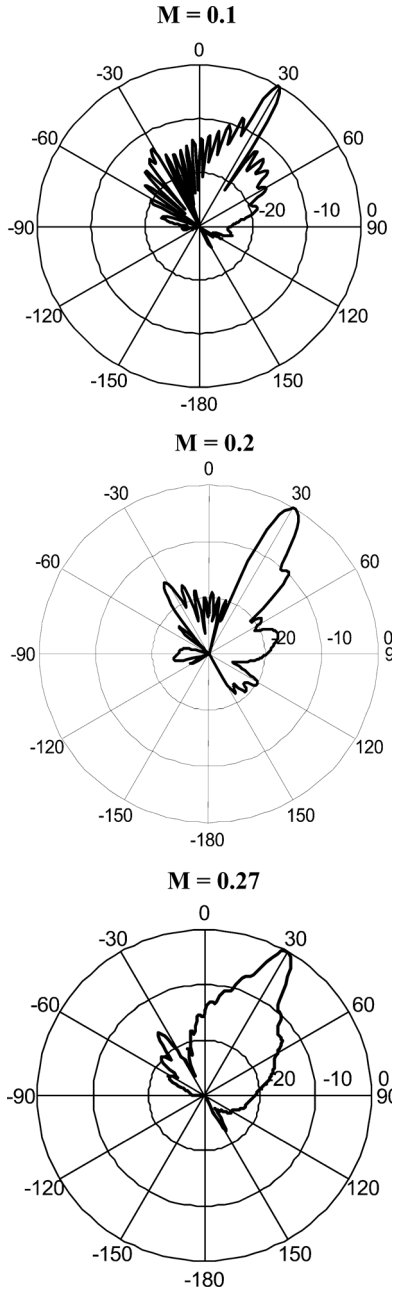

Fig. 20. Simulated E-plane radiation patterns for eight unit-cell leaky-wave antennas with different modulation factors.

gap size, copper strips were printed on a 2.54 mm thick substrate in order to achieve the impedance values necessary to implement the SMRS. This substrate, of approximately $\lambda_d/5$ thickness, was thick enough to introduce error into the sheet impedance approximation, used in Section III, which assumes an infinitely thin sheet. This error was due to elements interacting through the dielectric, resulting from the considerable thickness of the dielectric substrate. Even though excellent correspondence between the theoretical and simulated values of β is observed, disagreement between the theoretical and simulated value of α can be attributed to this source of error. Despite not being able to accurately predict α from SMRS theory, Table I presents full-wave simulation results that show that α can be controlled nearly independently of β by varying the modulation factor, M while keeping X and a fixed. Table I reports values of α and β extracted from full-wave simulation using periodic structure analysis for an antenna that is eight unit cells in length. Fig. 20 shows the simulated radiation patterns for the cases corresponding to Table I. The beam direction is approximately the same for all the radiation patterns but the beam width increases with increasing modulation. This confirms that the leakage rate can be controlled nearly independently of the phase constant.

TABLE I
EXTRACTED VALUES OF $\kappa = \beta - j\alpha$ FOR VARIOUS VALUES OF MODULATION FACTOR

M	β/k_0	α/k_0	κ (rad/m)	$\theta_{n=-1}$ (degrees)
0.1	1.568949	0.021147	328.6 - 4.42906j	29.3
0.2	1.568949	0.026375	328.6 - 5.52393j	30.0
0.27	1.574297	0.066588	329.7 - 13.9461j	30.1

VI. CONCLUSION

In this paper, a design procedure for a sinusoidally-modulated reactance surface (SMRS) allowing directive radiation at an arbitrary off-broadside angle is outlined. The implementation of the SMRS using printed metallic strips over a grounded dielectric substrate is also presented. An efficient method for determining the gap size between metallic strips is discussed. The design procedure allows for nearly independent control of the leakage rate and the phase constant along the antenna. A printed leaky-wave antenna based on the design procedure is reported. The antenna is directly fed and simple to fabricate. At the design frequency of 10 GHz, the antenna radiates at approximately 30° from broadside, and exhibits a gain of 18.4 dB. Good agreement between simulation and experiment has been observed. SMRS theory accurately predicted the phase constant β along the antenna, but the simulated attenuation constant differed due to the antenna's electrical thickness. Despite inaccuracy in the theoretical prediction of α due to the substrate thickness, it is shown through simulation that α can be controlled by varying the modulation factor without significantly perturbing β. This verifies the claim of nearly independent control of leakage rate and phase constant along the antenna.

REFERENCES

[1] D. R. Jackson and N. G. Alexopoulos, "Gain enhancement methods for printed-circuit antennas," *IEEE Trans. Antennas Propag.*, vol. 33, pp. 976–987, Sep. 1985.
[2] D. R. Jackson and A. A. Oliner, "A leaky-wave analysis of the high-gain printed antenna configuration," *IEEE Trans. Antennas Propag.*, vol. 36, pp. 905–910, Jul. 1988.
[3] A. P. Feresidis and J. C. Vardaxoglou, "High gain planar antenna using optimized partially reflective surfaces," *IEEE Trans. Antennas Propag.*, vol. 148, pp. 345–350, Dec. 2001.
[4] A. P. Feresidis, G. Goussetis, S. Wang, and J. C. Vardaxoglou, "Artificial magnetic conductor surfaces and their application to low-profile high-gain planar antennas," *IEEE Trans. Antennas Propag.*, vol. 53, pp. 209–215, Jan. 2005.
[5] C. Walter, *Traveling Wave Antennas*. New York: McGraw-Hill, 1965.
[6] A. A. Oliner and A. Hessel, "Guided waves on sinusoidally-modulated reactance surfaces," *IRE Trans. Antennas Propag.*, vol. 7, pp. 201–208, Dec. 1959.
[7] D. F. Sievenpiper, J. S. Colburn, B. H. Fong, J. J. Ottuschand, and J. L. Visher, "Holographic artificial impedance surfaces for conformal antennas," in *Proc. IEEE AP-S/URSI Int. Symp.*, Washington, DC, Jul. 20, 2005, vol. 1B, pp. 256–259.

[8] B. H. Fong, J. S. Colburn, P. R. Hertz, D. F. Sievenpiper, J. J. Ottusch, and J. L. Visher, "Polarization controlling holographic artificial impedance surfaces," in *Proc. IEEE AP-S Int. Symp.*, Jun. 2007, pp. 3824–3827.
[9] J. S. Colburn, A. Lai, and D. F. Sievenpiper, "Adaptive artificial impedance surface conformal antennas," in *Proc. IEEE AP-S Int. Symp.*, Jun. 1–5, 2009, pp. 1–4.
[10] C. Lee and H. Son, "Periodically slotted dielectrically filled parallel-plate waveguide as a leaky-wave antenna: E-polarization case," *IEEE Trans. Antennas Propag.*, vol. 47, pp. 171–178, Jan. 1999.
[11] J.-I. Lee, U.-H. Cho, and Y.-K. Cho, "Analysis for a dielectrically filled parallel-plate waveguide with finite number of periodic slots in its upper wall as a leaky-wave antenna," *IEEE Trans. Antennas Propag.*, vol. 47, pp. 701–706, Apr. 1999.
[12] J. Jacobsen, "Analytical, numerical, and experimental investigation of guided waves on a periodically strip-loaded dielectric slab," *IEEE Trans. Antennas Propag.*, vol. 18, pp. 370–388, May 1970.
[13] A. M. Patel and A. Grbic, "A printed leaky-wave antenna with a sinusoidally modulated surface reactance," in *Proc. IEEE AP-S Int. Symp.*, Jun. 1–5, 2009, pp. 1–4.
[14] R. Collin and F. Zucker*, Antenna Theory, Part II*. New York: McGraw-Hill, 1969.
[15] J. S. Colburn, D. F. Sievenpiper, B. H. Fong, J. J. Ottuschand, J. L. Visher, and P. R. Herz, "Advances in artificial impedance surface conformal antennas," in *Proc. IEEE AP-S/URSI Int. Symp.*, Jun. 9–15, 2007, pp. 3820–3823.
[16] M. Guglielmi and D. R. Jackson, "Broadside radiation from periodic leaky-wave antennas," *IEEE Trans. Antennas Propag.*, vol. 41, pp. 31–37, Jan. 1993.
[17] S. Maci, A. Cucini, and M. Casaletti, "A pole-zero matching method for EBG surfaces composed of a dipole FSS printed on a grounded dielectric slab," *IEEE Trans. Antennas Propag.*, vol. 53, pp. 70–81, Jan. 2005.
[18] S. Tretyakov*, Analytical Modeling in Applied Electromagnetics*, 2nd ed. Englewood Cliffs, NJ: Prentice-Hall, 1968.

Amit M. Patel (S'06) received both the B.S.E. degree in electrical engineering and the B.S. degree in physics from Michigan State University, East Lansing, in 2007, and the M.S.E. degree in electrical engineering from the University of Michigan, Ann Arbor, in 2009, where he is currently working toward the Ph.D. degree.

His research interests include periodic structures, metamaterials, leaky-wave antennas, and tensor surfaces.

Mr. Patel received the Best Student Paper Award at the IEEE International Symposium on Antennas and Propagation in 2009. In 2010, he was the recipient of the Science, Mathematics and Research for Transformation (S.M.A.R.T) Scholarship sponsored by the U.S. Department of Defense.

Anthony Grbic (S'00–M'06) received the B.A.Sc., M.A.Sc., and Ph.D. degrees in electrical engineering from the University of Toronto, ON, Canada, in 1998, 2000, and 2005, respectively.

In January 2006, he joined the Department of Electrical Engineering and Computer Science, University of Michigan, Ann Arbor, where he is currently an Assistant Professor. His research interests include engineered electromagnetic structures (metamaterials, electromagnetic bandgap materials, frequency selective surfaces), printed antennas, microwave circuits and analytical electromagnetics.

Dr. Grbic received the Best Student Paper Award at the 2000 Antenna Technology and Applied Electromagnetics Symposium and an IEEE Microwave Theory and Techniques Society Graduate Fellowship in 2001. In 2008, he was the recipient of an AFOSR Young Investigator Award as well as an NSF Faculty Early Career Development Award. In January 2010, he was awarded a Presidential Early Career Award for Scientists and Engineers.